Effect of Island Geometry on the Replay Signal in Patterned Media Storage

Paul W. Nutter, David McA. McKirdy, Barry K. Middleton, *Member, IEEE*, David T. Wilton, and Hazel A. Shute

***Abstract*—In a move to extend the storage capabilities of magnetic storage systems beyond 1 Tb/in^2, the use of patterned media has often been cited. Here, recorded domains are constrained by the geometry of the magnetic island and not the geometry of the recording head. Conventional two-dimensional readout modeling techniques, using the reciprocity integral, rely on the assumption that the across-track medium magnetization is uniform under the giant magnetoresistive replay head. However, in the case of a geometrically constrained medium this is not the case. This paper investigates the effect that the island geometry has on the characteristics of the replay signal in perpendicular patterned magnetic media storage through the extension of the reciprocity integral to three dimensions. The paper describes replay pulses that offer different characteristics from those obtained by conventional two-dimensional techniques. The origins of these differences are explained by the variation in medium magnetization across the track.**

***Index Terms*—Magnetic recording, patterned media, perpendicular magnetization, reciprocity.**

I. Introduction

In THE QUEST for reliable ultrahigh-density magnetic storage media, the use of patterned media is widely recognized as offering the potential to overcome some of the physical limitations imposed on conventional continuous magnetic media. Increased storage density in continuous media requires the recorded transitions to be packed as close together as possible without having any detrimental effect on the system performance in terms of replay signal-to-noise ratio (SNR) and, hence, bit-error rate (BER). Replay SNR is affected by many factors, including transition noise and bit shifts due to strong intergranular magnetic coupling [1]. In addition, increased storage density can result in a reduced number of magnetic grains per bit, which in turn results in increased media noise and poor SNR. In order to maintain an acceptable level of SNR in high-density systems, a reduction in grain size is required such that there are a sufficient number of grains per bit. However, studies have shown that a reduction in magnetic grain size can lead to increased thermal instability [2], [3], leading to the random magnetization of the magnetic particles; the so-called superparamagnetic limit [4]–[6].

Manuscript received May 28, 2004; revised July 16, 2004. This work was supported in part by the Engineering and Physical Sciences Research Council, U.K., under Grant GR/R63479.

P. W. Nutter, D. McA. McKirdy, and B. K. Middleton are with the Department of Computer Science, The University of Manchester, Manchester M13 9PL, U.K. (e-mail: p.nutter@man.ac.uk; mckirdy@cs.man.ac.uk; b.k.middleton@cs.man.ac.uk).

D. T. Wilton and H. A. Shute are with the School of Mathematics and Statistics, University of Plymouth, Plymouth PL4 8AA, U.K. (e-mail: d.wilton@plymouth.ac.uk; h.shute@plymouth.ac.uk).

Digital Object Identifier 10.1109/TMAG.2004.835697

Magnetic media are constantly being refined in order to extend the limits of continuous media. For example, the introduction of antiferromagnetically coupled (AFC) longitudinal media [7], and a potential move to perpendicular media [8], have demonstrated improved storage capabilities. However, such techniques still offer limited storage density due to the physical limitations of continuous media. An alternative approach that offers vastly improved storage densities, while overcoming the physical limitations imposed on continuous media, is the use of patterned magnetic media [6], [9]. In a patterned medium, each data bit is recorded to an isolated, submicrometer-size magnetic island, which is magnetized longitudinally or perpendicularly [6], [10], [11]. Since each island acts as a single bounded domain, the grains are strongly coupled, and consequently the grain size need not be reduced and each island can theoretically contain a single magnetic grain and still remain thermally stable [9]. Furthermore, transition noise, due to magnetic coupling between recorded marks, is effectively removed as a result of the nonmagnetic barrier between islands, resulting in an overall reduction in media noise and improved replay SNR [6].

While much attention has been paid to the fabrication of patterned media, little attention has been focused on the readout and recovery of data from such media. Some researchers have analyzed the replay process in patterned media systems. Here, work has concentrated mainly on longitudinal media [12], [13] or analysis has been performed using conventional two-dimensional (2-D) approaches to replay modeling [14], [15], using the reciprocity integral [1], [16]. However, when analyzing the replay process in ultrahigh-density storage systems, such as patterned media, it is essential that accurate models of the replay process are utilized, otherwise subsequent analysis, such as the design of the data recovery channel, may be inaccurate.

In the case of conventional replay modeling techniques, it is often assumed that both media magnetization and the head field are uniform across the data track (infinite width approximation); in this case, the reciprocity integral may be expressed as a function of the scan direction only [16]. However, in the case of patterned media, the shape of the recorded magnetic mark is constrained by the geometry of the patterned island and not the recording head. Hence, the assumption that the medium magnetization is uniform under the replay head is invalid, since the width of the patterned element may be comparable or even less than the track width of the (typically) giant magnetoresistive (GMR) sensor. In order to accurately predict the form of the readout signal, analysis needs to be performed over three-dimensional (3-D) space. Here, we present a thorough analysis of the replay process from perpendicular patterned

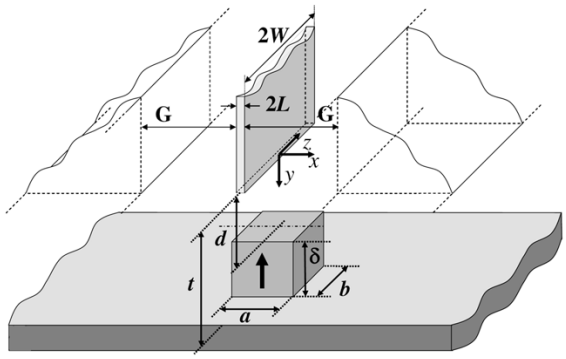

Fig. 1. Geometry of the shielded GMR head structure and patterned magnetic medium.

media using conventional GMR replay heads. The analysis predicts the replay response to an isolated magnetic island and takes into account the effects of the geometrically constrained media through the use of a 3-D evaluation of the reciprocity integral. This paper is organized as follows. In Section II, conventional replay modeling techniques are discussed and the proposed 3-D reciprocity approach is introduced. In Section III, the results produced using the 3-D model are analyzed in terms of the characteristics of the response due to an isolated magnetic island. In Section IV, conclusions are drawn as to the effect of the island geometry on the characteristic of the replay pulse in patterned media using conventional GMR heads.

II. Replay Modeling

Fig. 1 illustrates the 3-D geometry for the shielded GMR head and the patterned magnetic medium being modeled.

Here, the GMR element (of unit reciprocity potential) is of length $2L$ (along-track direction x), width $2W$ (across-track direction z), of semi-infinite height, and lies a distance d above the surface of the patterned magnetic medium, of thickness δ, and a distance t above any (semi-infinite) magnetic soft underlayer (SUL) of infinite permeability. In the case of a medium with an SUL, no interlayer is assumed, i.e., $t = d + \delta$. The side shields are assumed to be of infinite width (across-track direction), of semi-infinite height, and separated from the GMR element by gaps of width G; the total shield-to-shield separation being $2(L + G)$. In the rectangular coordinate system adopted, the along-track direction is x, the across-track direction is z, and y is the vertical position under the air-bearing surface (ABS) of the GMR head. The midpoint of the GMR sensor element along the ABS is assumed to be the coordinate origin.

The replay voltage signal due to any change in magnetization in the recording medium can be derived using the reciprocity integral [1]. In the case of a GMR head, the voltage signal is simply proportional to the signal flux injected into the GMR sensor at the ABS. In this simple (2-D) case, the signal flux in the GMR sensor when the medium is at position $\bar{x}(= vt)$ is given by the scalar correlation integral [16]

$$\Phi_{\text{sig}}(\bar{x}) = \mu_o W_t \int_{-\infty}^{\infty} dx \int_{d}^{d+\delta} dy H_y(x,y) M_y(x-\bar{x}) \qquad (1)$$

where M_y is the perpendicular magnetization component of the medium which varies in x only, H_y is the head sensitivity function, W_t is the effective track width (i.e., where M_y is nonzero), and μ_o is the permeability of free space.

Since the head sensitivity function is related to the differential of the scalar magnetic field potential ϕ, then the reciprocity formula may be expressed in the form

$$\Phi_{\text{sig}}(\bar{x}) = \mu_o W_t \int_{-\infty}^{\infty} \left[\int_{d}^{d+\delta} -\frac{\partial \phi(x,y)}{\partial y}\, dy \right] M_y(x-\bar{x})\, dx. \quad (2)$$

Evaluating the integral over y gives

$$\Phi_{\text{sig}}(\bar{x}) = \mu_o W_t \left\{ \int_{-\infty}^{\infty} \phi(x,d) \cdot M_y(x-\bar{x})\, dx - \int_{-\infty}^{\infty} \phi(x,d+\delta) \cdot M_y(x-\bar{x})\, dx \right\} \quad (3)$$

and identifying that the integrals in (3) are correlation integrals $(\times)$ gives

$$\Phi_{\text{sig}}(\bar{x}) = \mu_o W_t \{ [M_y(x) \times \phi(x,d)] - [M_y(x) \times \phi(x,d+\delta)] \}. \quad (4)$$

Hence, the reciprocity formula for the GMR head may be expressed in the form

$$\Phi_{\text{sig}}(\bar{x}) = \mu_o W_t \{ \text{IFT}[\hat{M}_y^*(k_x) \cdot \hat{\phi}(k_x,d)] - \text{IFT}[\hat{M}_y^*(k_x) \cdot \hat{\phi}(k_x,d+\delta)] \} \quad (5)$$

where M_y: $\hat{M}_y$ and ϕ: $\hat{\phi}$ are Fourier transforms pairs, $\hat{M}_y^*$ is the complex conjugate of $\hat{M}_y$, IFT is the inverse Fourier transform operation, and k_x is the Fourier transform wavenumber in x.

To derive the signal flux in the GMR sensor due to any magnetization change in the medium, the scalar potential distributions at the top $(y = d)$ and the bottom $(y = d + \delta)$ of the magnetic medium need to be determined. A number of techniques for predicting the scalar magnetic potential distribution are documented. In the case of no SUL present, an expression commonly used is that of Potter [17], whereby the GMR head is considered to be two inductive Karlqvist heads. In this case, the potential along the ABS $(y = 0)$ can be expressed as a linear variation of the potential from the sensor to the side shield across the gap, i.e.,

$$\phi(x,0) = \begin{cases} 1 & 0 \le |x| \le L \\ \dfrac{L+G-|x|}{G} & L < |x| < L+G \\ 0 & |x| \ge L+G \end{cases}. \qquad (6)$$

A more accurate ABS approximation is that of Ruigrok [18], who proposed the equally weighted sum of a linear potential and the potential of an infinitely thin head, whereby, the linear variation in potential across the gap is modified to include a curvature term, i.e.,

$$\phi(x,0) = \begin{cases} 1 & 0 \le |x| \le L \\ \dfrac{L+G-|x|}{2G} + \dfrac{1}{\pi} \arcsin\left(\dfrac{L+G-|x|}{G}\right) & L < |x| < L+G \\ 0 & |x| \ge L+G \end{cases}. \qquad (7)$$

Using either of these expressions, the potential at any point y below the ABS can be easily calculated using the well-known spacing loss expression [1]

$$\hat{\phi}(k_x, y) = \hat{\phi}(k_x, 0)\exp(-k_x y). \tag{8}$$

While these approximations can produce reliable results, they do not take into account the effect that any SUL present has upon the replay process. As an approximation, the effect of the SUL may be introduced by considering the sensitivity function of the replay head and the sensitivity function of the replay head image in the SUL [19]. Other, more accurate, approaches involve the calculation of the potential distribution below the ABS with an SUL present. For example, in [20], the effect of the SUL is introduced through a weighted sum of the potential variation between the pole corner and the *SUL*, rather than between the pole corner and the *shield*. In [21], an explicit ABS potential function is given which is in the style of (7) but has three parameters. These parameters, which depend on the ratio t/G, are determined from a finite-element model. Both of these techniques have been shown to produce very accurate results; however, neither are appropriate in three dimensions where track edge effects are significant, since they provide no potential variation in the across-track direction.

In the case of a patterned medium, the size and shape of the recorded domains are constrained by the geometry of the magnetic island. In this situation, a more accurate replay model is required which takes into account variation in magnetization in both the along-track (x) and across-track (z) directions; this requires the extension of the reciprocity integral over 3-D space.

The reciprocity integral of (1) can be easily extended into 3-D space by reintroducing the across-track coordinate z, i.e.,

$$\Phi_{\text{sig}}(\bar{x}) = \mu_o \int_{-\infty}^{\infty}\int_{-\infty}^{\infty}\left[\int_{d}^{d+\delta} -\frac{\partial\phi(x,y,z)}{\partial y}\,dy\right] \times M_y(x-\bar{x},z)\,dx\,dz \tag{9}$$

which gives

$$\Phi_{\text{sig}}(\bar{x}) = \mu_o\{\text{IFT}[\hat{M}_y^*(k_x,k_z)\cdot\hat{\phi}(k_x,d,k_z)] - \text{IFT}[\hat{M}_y^*(k_x,k_z)\cdot\hat{\phi}(k_x,d+\delta,k_z)]\}. \tag{10}$$

The signal flux is now dependent on the 3-D potential distribution at the top and the bottom of the magnetic medium and the magnetization distribution in the medium. Equation (10) takes into account the magnetization variation across the width of the medium, rather than simply along the track as in standard 2-D approaches [17], [18].

In order to predict the potential distribution at any point below the plane of the ABS of a GMR head, the approach described in detail in [22] is followed. There, a technique for predicting the 3-D head field for a perpendicular magnetic recording head with an SUL is proposed. The method initially assumes forms for the variation in the scalar magnetic potential between the GMR sensor and the SUL and between the side shields and the underlayer, based on the 2-D approximations developed in [20]. Fourier techniques are then employed to give an exact solution to this simplified approximate problem, and in particular the solution in the plane of ABS is found. If the ABS lies in the plane $y = 0$ and the SUL is at $y = t$, the Fourier transforms of the potentials, $\phi(x, y, z)$, in these planes are related by [1]

$$\hat{\phi}(k_x, y, k_z) = \hat{\phi}(k_x, 0, k_z)\frac{\sinh(\kappa(t-y))}{\sinh(\kappa t)} \tag{11}$$

where $\kappa = \sqrt{k_x^2 + k_z^2}$ and k_x and k_z are the wavenumbers in the x (along-track) and z (across-track) directions, respectively. The resulting potential in any plane below the ABS can thus be predicted using Fourier transform operations. Equation (11) partially corrects the approximate potentials originally assumed under the GMR sensor and shields.

In the case of no SUL, we use the above method but with a large, but finite, value of t to predict the ABS potential (for large t relative to the shield-to-shield separation the underlayer is effectively an infinite distance away from the replay head). Equation (11) is then taken with t infinite to give the familiar exponential spacing loss of [1]

$$\phi(k_x, y, k_z) = \hat{\phi}(k_x, 0, k_z)\exp(-\kappa y). \tag{12}$$

TABLE I
GMR HEAD DIMENSIONS

Dimensions (nm)	GMR1	GMR2
$2W$	40, (80, 160)	120
$2L$	8	4
$2(L+G)$	32	88

III. REPLAY PULSE ANALYSIS

In order to understand how the island geometry affects the replay signal characteristics, the replay pulse due to an isolated magnetic island has been investigated using the two GMR head structures listed in Table I. These head dimensions have been taken from designs proposed for future ultrahigh-density applications [23]–[25]. The pulse responses have been generated using the approaches described in Section II, assuming a single isolated magnetic island of single domain and perpendicular magnetization. The volume surrounding the island is assumed to be free-space.

Figs. 2 and 3 illustrate simulated replay responses to an isolated magnetic island of length $a = 50$ nm using the replay head structure of GMR1, for a head width of $2W = 40$ nm and a head-to-medium separation of $d = 10$ nm. The responses were generated from the analysis in Section II, using the 2-D (Ruigrok) and 3-D approaches (where the island is assumed to be square). Fig. 2 illustrates the case of no SUL present for (a) a thin film ($\delta = 20$ nm) and (b) a thick film ($\delta = 100$ nm). Fig. 3 illustrates the case of an SUL present below the magnetic film for (a) a thin film ($\delta = 20$ nm) and (b) a thick film ($\delta = 100$ nm). In the case of the 2-D analysis, the potential below the ABS was calculated using the 2-D equivalent of (11), i.e., in x only, when an SUL is present.

In the case of the 2-D modeling approaches, Potter (not shown) and Ruigrok, identical responses are observed. However, in the case of the 3-D approach, where the across-track variation of magnetization is taken into account, a difference in pulse shape is clearly observed, particularly in the no SUL case.

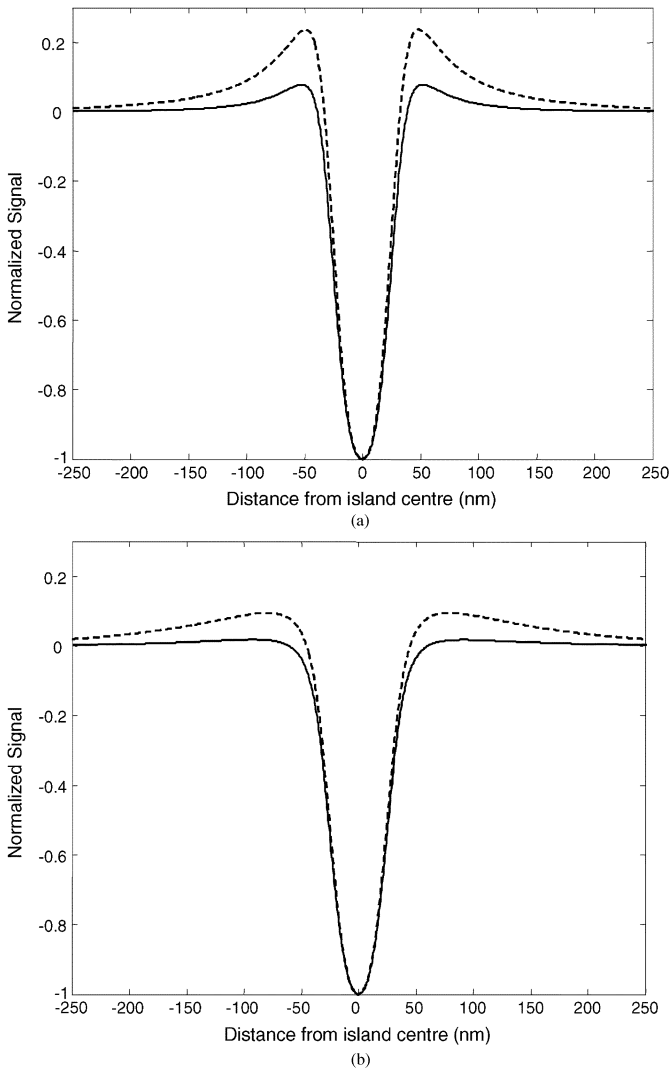

Fig. 2. Simulated pulse responses due to an isolated island of length $a = 50$ nm, using 2-D Ruigrok (dashed line) and 3-D (solid line) approaches for (a) a thin film ($\delta = 20$ nm) and (b) a thick film ($\delta = 100$ nm), with no SUL present, using the head structure of GMR1.

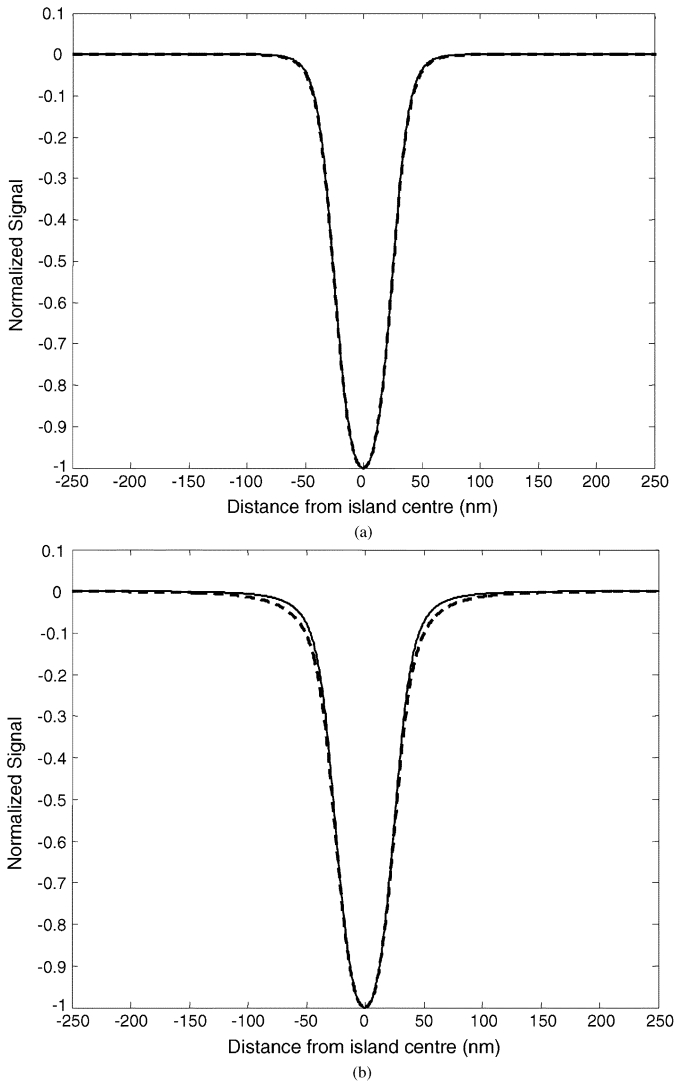

Fig. 3. Simulated pulse responses due to an isolated island of length $a = 50$ nm, using 2-D Ruigrok (dashed line) and 3-D (solid line) approaches for (a) a thin film ($\delta = 20$ nm) and (b) a thick film ($\delta = 100$ nm) with an SUL immediately below the patterned magnetic film, using the head structure of GMR1.

In the no SUL case, the 2-D pulse in particular is characterized by the presence of large overshoots either side of the main pulse. This "triplet" pulse shape arises due to the opposite charges present at the top and bottom surfaces of the magnetic islands. The charge along the bottom surface introduces a broad pulse of opposite polarity and reduced amplitude to the pulse introduced by the charge along the top surface [14]. In the case of a medium with an SUL present, the charge along the bottom surface of the medium is shifted further away from the head by the presence of the SUL, and its resulting contribution to the shape of the replay pulse response is insignificant; as a consequence, the overshoots are removed, as evident in Fig. 3.

In the case of a medium with no SUL, it can be seen in Fig. 2 that for the 2-D modeling, the amount of overshoot present in the replay pulse is significantly overestimated compared with the responses generated using the 3-D approach. In the case of a thick medium [Fig. 2(b)], the 3-D model predicts that these overshoots are effectively removed; whereas the 2-D approaches still predict a considerable contribution. This result is interesting, since channel studies have shown that the presence of these overshoots gives rise to a degraded performance (in terms of BER) from the replay channel [14].

In the case of a medium with an SUL (Fig. 3), no significant difference is observed between the 2-D and 3-D approaches, although some (slight) difference is observed as the film thickness increases [Fig. 3(b)]. A similar result was observed in the analysis of GMR2 for the same size island (although the pulse responses produced using the two head structures differed slightly in shape). The reason for the similarity between the results produced using the 2-D and 3-D approaches can be easily explained. With an SUL present, the magnetic field below the ABS of the GMR head is focused within a narrow area centered below the sensor element. However, when there is no SUL present, the magnetic field is spread over a wider area and so the edges of the islands have a much greater influence on the readback performance. Hence, we can conclude that in the case of a medium with no SUL present, the finite width of the

island affects predominantly the amount of overshoot present in the replay pulse. In the case of a medium with an SUL, the finite island width has little effect due to the removal of the overshoots by the presence of the SUL itself.

It is well known that the use of an SUL improves the writing performance by providing a large field gradient through the magnetic medium [26]. While the presence of the SUL results in an increased readback signal amplitude (borne out using the described model), theoretical observations show that the resulting pulse response is in fact wider than the corresponding case with no SUL present. Using the GMR head structure of GMR1 for a 50 nm square island, the pulsewidth (PW_{50}) is 47.9 nm with no SUL present and 52.1 nm with an SUL ($\delta = 20$ nm, $d = 10$ nm, no interlayer in the SUL case). These results are in agreement with published results, which also show that the use of an SUL has a detrimental effect on the readback performance, particularly at high densities [27], [28].

The origins of the variation in shape of the pulse responses generated using the 3-D approach, in particular the amount of pulse overshoot, can be further investigated by analyzing the response to a rectangular island of varying width b. Fig. 4(a) illustrates pulse responses for an isolated island of length $a = 50$ nm, ($d = 10$ nm, $\delta = 20$ nm) with no SUL present for varying bit width b of 50 nm (square island), 150, 300, and 600 nm (rectangular). Also illustrated is the 2-D response (Ruigrok) to an island of length 50 nm (assumed infinite width).

It is evident from Fig. 4 that as the width of the island becomes large compared with the width of the GMR sensor ($2W = 40$ nm for GMR1), the shape of the resulting pulse response approaches that produced using the 2-D approaches (in this case Ruigrok). A similar result was also observed when using the head structure of GMR2, as illustrated in Fig. 4(b).

Thus, it can be concluded that the difference in the response arises due to the finite track width imposed by the geometry of the magnetic island; in such cases, the 2-D approximations, which assume constant magnetization across track under the head, are inaccurate.

To further this investigation, we analyzed how the width of the GMR sensor element affects the pulse shape. Fig. 5 illustrates pulse responses due to an isolated island of length $a = 50$ nm and width $b = 50$ nm (square), with no SUL present, for varying GMR sensor width, $2W$, using the head structure of GMR1. Also illustrated is the pulse response obtained using the 2-D approach (Ruigrok).

It can be seen that as the head width is increased (from a size comparable to the fixed size of the island), then the shape of the resulting pulse response approaches that of the 2-D approximations (as previously for a fixed head width and increased island width). Further analysis shows that for a very large bit width b, the pulse response is always the same as that obtained using the 2-D approaches, irrespective of the GMR sensor width; this result is in agreement with previous results presented.

Since these results appear to indicate that the bit width is the major factor affecting the shape of the replay pulse (with no SUL), further analysis was performed to investigate how the bit width affects the shape of the replay pulse in terms of the pulsewidth (PW_{50}) and percentage overshoot (with respect to the peak amplitude) for both GMR heads.

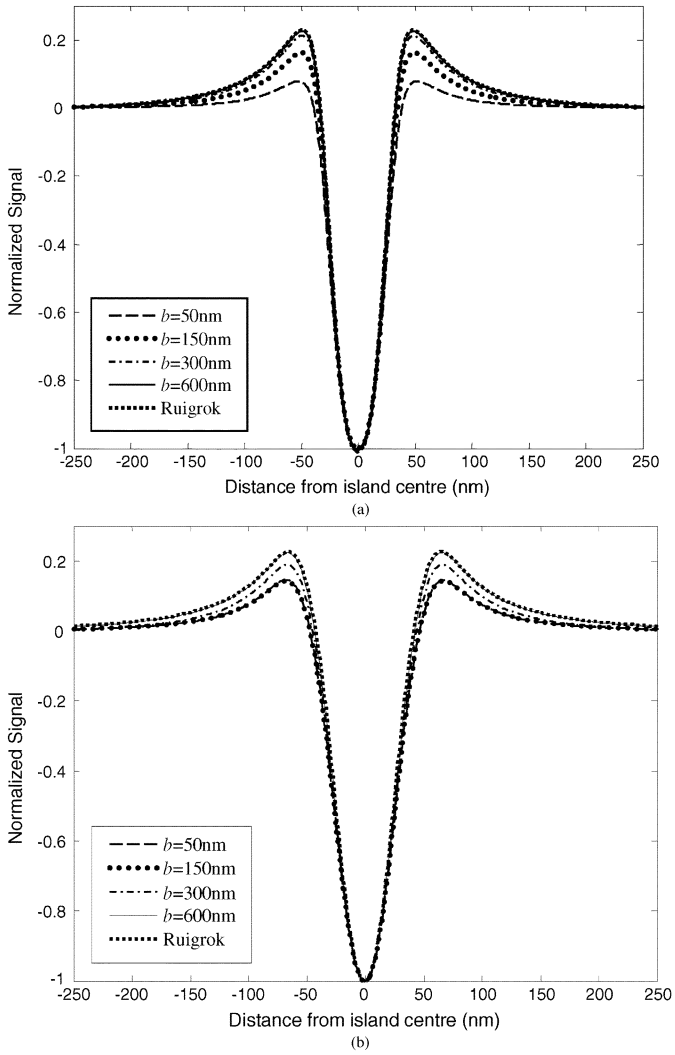

Fig. 4. Simulated pulse responses due to an isolated island of length $a = 50$ nm and varying width, with no SUL present, using the head structures of (a) GMR1, and (b) GMR2.

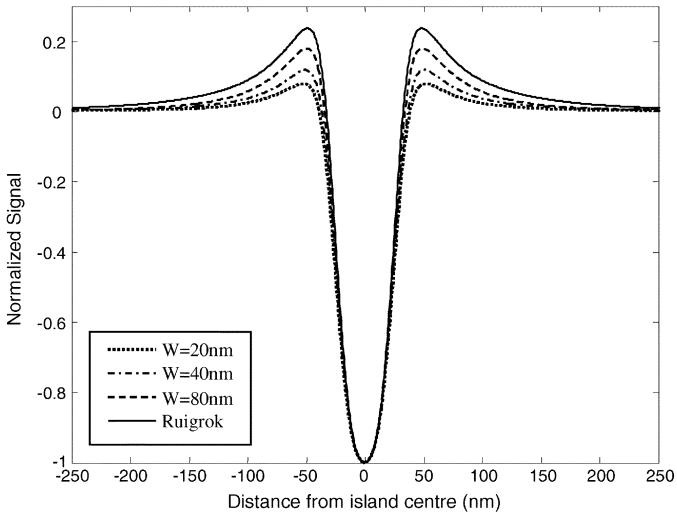

Fig. 5. Simulated pulse responses due to an isolated island of length $a = 50$ nm and width $b = 50$ nm, with no SUL present, for varying GMR sensor width $2W$, using the head structure of GMR1.

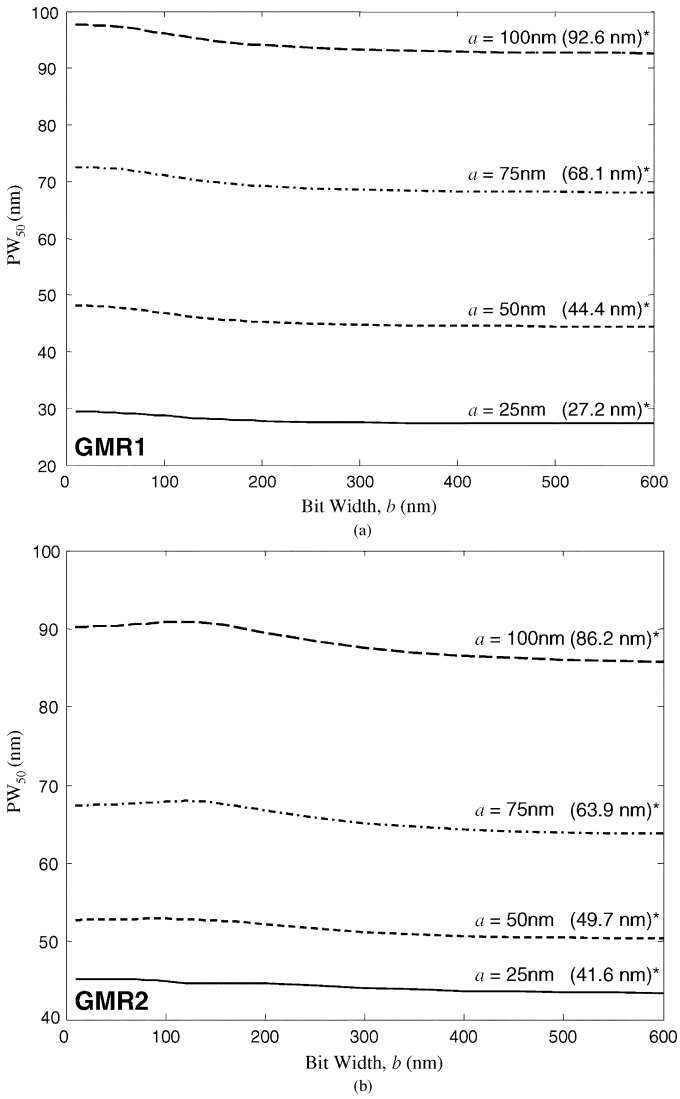

Fig. 6. Comparison of pulsewidth (PW_{50}) against bit width b for varying bit length a using the head structures of (a) GMR1 and (b) GMR2. (* indicates the pulsewidth measured from the responses generated using the 2-D Ruigrok approximation).

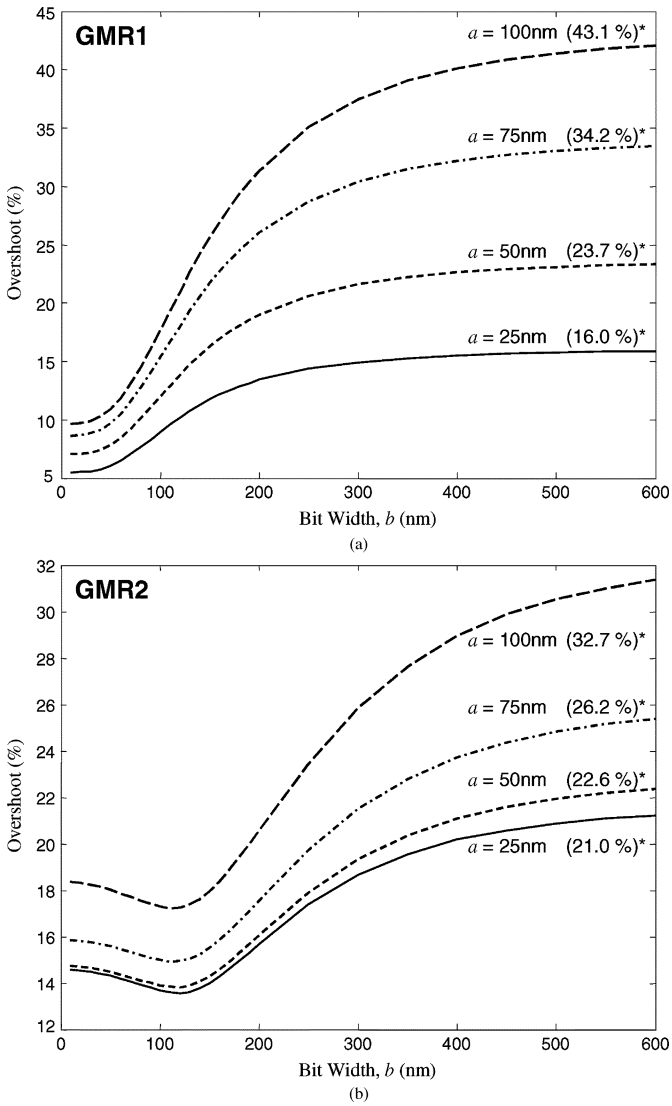

Fig. 7. Comparison of percentage overshoot (%), with respect to the absolute peak amplitude of the pulse, against bit width b for varying bit length a using the head structures of (a) GMR1 and (b) GMR2 (asterisk indicates the percentage overshoot measured from the responses generated using the 2-D Ruigrok approximation).

Fig. 6 illustrates pulsewidth PW_{50} (nm) versus bit width b at four different island lengths of $a = 25$, 50, 75, and 100 nm for GMR1 in Fig. 6(a) ($2W = 40$ nm) and GMR2 in Fig. 6(b) when no SUL is present. From Fig. 6, it can be seen that the pulsewidth appears slightly larger for small bit widths, and in the case of GMR2 [Fig. 6(b)], this reaches a peak when the bit width is the same as the width of the GMR sensor, $b = 2W = 120$ nm. Overall, the effect of the island width on the pulsewidth is very small. For large bit widths, the pulsewidth approaches that measured using the 2-D approaches (shown in brackets). In the case of a patterned medium with an SUL present, a slight difference in pulsewidth is observed as the island width is varied; but this differs little from the pulsewidth obtained using conventional 2-D approaches for the same island length.

Fig. 7 illustrates percentage overshoot (with respect to the absolute peak amplitude) versus bit width b at four different bit lengths of $a = 25$, 50, 75, and 100 nm for GMR1 in Fig. 7(a) ($2W = 40$ nm) and GMR2 in Fig. 7(b).

As the bit length is increased a corresponding increase in the amount of overshoot is observed; this is what would be expected as the island length increases and the dipulses produced at each edge of the bit along the track interfere less. However, what is evident from Fig. 7 is that the amount of overshoot in the resulting response is dependent upon the width of the island. In the case of GMR2 [Fig. 7(b)], the minimum overshoot is observed when the island width is comparable to the width of the sensor element, $b = 2W = 120$ nm. Again, for large bit widths the percentage overshoot approaches that measured using the 2-D approaches (shown in brackets).

The many patterning options available for the production of patterned media permit a wide variation in the array period, island size, and island shape. In particular, most patterning techniques will produce square or circular islands over a regular array. In order to investigate how the shape of the island (as a consequence of the lithographic process employed) affects the

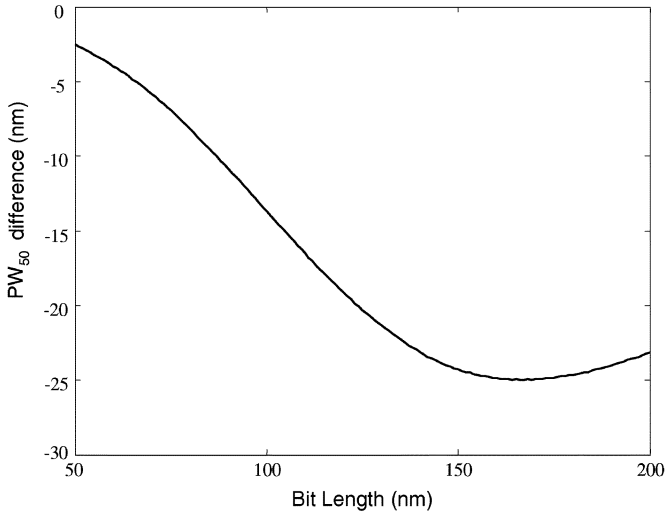

Fig. 8. Plot of the difference in pulsewidth produced by a circular and square island against island length using the head structure of GMR2.

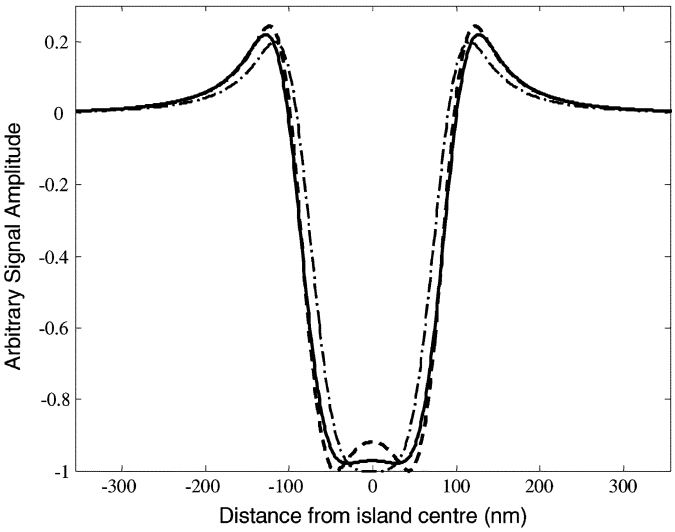

Fig. 9. Simulated pulse responses due to a 168-nm-diameter circular island (dashed-dotted line), a 168-nm square island (dashed line) and a 190-nm-diameter circular island (solid line).

replay pulse shape, the difference in pulsewidth produced from a circular and square island for varying bit length a was determined as illustrated in Fig. 8, using the replay head structure GMR2.

The overall effect on the pulse response in this case is a reduction in the pulsewidth for a circular mark; this result is sensible considering the reduction in magnetic material along the island edge due to the circular geometry. A peak difference is observed when the island size is approximately 168 nm; at this point the pulse shapes are quite different, as illustrated in Fig. 9, where the pulse responses have not been normalized. It should be noted that round and square islands of equal dimensions will exhibit different magnetic properties. Also illustrated in Fig. 9 is the pulse response due to a round island of diameter 190 nm; this island has a surface area identical to that of the 168 nm square island. It is evident that the pulse shape is strongly dependent upon the size and shape of the island. While this effect is most dramatic at large bit lengths, it may become more evident as storage densities increase toward the goal of 1 Tb/in^2, where reduced replay head geometries may be required.

IV. Conclusion

A 3-D evaluation of the reciprocity integral has been developed and used to analyze the characteristics of the replay response from patterned media storage using perpendicular magnetic media. It has been shown that in the case of a medium with an SUL, the shape of the replay pulse is largely independent of the width of the island. However, in the case of a perpendicular medium with no SUL, the characteristics of the pulse response depend largely on the shape of the magnetic island, in particular its width. For a constant bit length, it has been shown that as the bit width becomes very large compared to the width of the GMR read head sensor element, the resulting response becomes similar to the response generated using conventional 2-D approaches (Potter and Ruigrok). A similar result is observed as the GMR sensor width is increased for a fixed bit width. However, in the case where the island width is comparable to the width of the head sensor element width, the amount of overshoot present in the isolated response is overestimated using conventional 2-D approaches. In particular, the minimum overshoot is observed when the island width is the same as the width of the sensor element. However, analysis has shown that at this point the pulsewidth is also at its greatest. Hence, a compromise must be made between the pulsewidth required and the amount of overshoot that can be tolerated, i.e., by the channel electronics.

Since the width of the island in patterned media affects the shape of the resulting replay pulse for the case of a perpendicular media with no SUL present, a 3-D replay model must be used in order to accurately predict the resulting replay pulse shape. Such a model is essential in the situation where the width of the replay sensor becomes comparable to the bit width, as in future ultrahigh-density applications.

Further work will include the extension of this analysis to model sensor characteristics, such as sensor efficiency, which will permit a thorough investigation of replay amplitude and SNR characteristics. In addition, due to the flexible nature of the 3-D model described, the effect of off-track reading in patterned media storage, and its effect on the performance of the Viterbi read channel will be investigated.

References

[1] H. N. Bertram, *Theory of Magnetic Recording*, Cambridge, UK: Cambridge Univ. Press, 1994.

[2] S. H. Charap, P.-L. Lu, and Y. He, "Thermal stability of recorded information at high densities," *IEEE Trans. Magn.*, vol. 33, pp. 978–983, Jan. 1997.

[3] Y. Zhang and H. N. Bertram, "Thermal decay in high density disk media," *IEEE Trans. Magn.*, vol. 34, pp. 3786–3793, Sept. 1998.

[4] D. Weller and A. Moser, "Thermal effect limits in ultrahigh-density magnetic recording," *IEEE Trans. Magn.*, vol. 35, pp. 4423–4437, Nov. 1999.

[5] Y. Zhang and H. N. Bertram, "Thermal decay of signal and noise in high-density thin-film media," *IEEE Trans. Magn.*, vol. 35, pp. 4326–4338, Sept. 1999.

[6] R. L. White, R. M. H. New, and R. F. W. Pease, "Patterned media: A viable route to 50 Gbit/in^2 and up for magnetic recording?," *IEEE Trans. Magn.*, vol. 33, pp. 990–995, Jan. 1997.

[7] H. J. Richter, "How antiferromagnetic coupling can stabilize recorded information," *IEEE Trans. Magn.*, vol. 38, pp. 1867–1872, Sept. 2002.
[8] A. Moser, K. Takano, D. T. Margulies, M. Albrecht, Y. Sonobe, Y. Ikeda, S. Sun, and E. E. Fullerton, "Magnetic recording: Advancing into the future," *J. Phys. D, Appl. Phys.*, vol. 35, no. 19, pp. R157–R167, 2002.
[9] R. L. White, "The physical boundaries to high-density magnetic recording," *J. Magn. Magn. Mater.*, vol. 209, pp. 1–5, 2000.
[10] Y. Chou and P. R. Krauss, "Quantum magnetic disk," *J. Magn. Magn. Mater.*, vol. 155, pp. 151–153, 1996.
[11] G. F. Hughes, *Patterned Media, the Physics of Ultra-High-Density Magnetic Recording*, M. L. Plumer, J. van Ek, and D. Weller, Eds. Berlin, Germany: Springer-Verlag, 2001, ch. 7.
[12] S. K. Nair and R. M. H. New, "Patterned media recording: Noise and channel equalization," *IEEE Trans. Magn.*, vol. 34, pp. 1916–1918, July 1998.
[13] J.-G. Zhu, X. Lin, L. Guan, and W. Messner, "Recording, noise, and servo characteristics of patterned thin film media," *IEEE Trans. Magn.*, vol. 36, pp. 23–29, Jan. 2000.
[14] G. F. Hughes, "Read channels for patterned media," *IEEE Trans. Magn.*, vol. 35, pp. 2310–2312, Sept. 1999.
[15] ——, "Read channels for prepatterned media with trench playback," *IEEE Trans. Magn.*, vol. 39, pp. 2564–2566, Sept. 2003.
[16] S. X. Wang and A. Taratorin, *Magnetic Information Storage Technology*. New York: Academic, 1999.
[17] R. I. Potter, "Digital magnetic recording theory," *IEEE Trans. Magn.*, vol. MAG-10, pp. 502–508, Sept. 1974.
[18] J. J. M. Ruigrok, *Short-Wavelength Magnetic Recording: New Methods and Analyses*. Oxford, U.K.: Elsevier, 1990.
[19] S. Khizroev and D. Litvinov, "Parallels between playback in perpendicular and longitudinal recording," *J. Magn. Magn. Mater.*, vol. 257, pp. 126–131, 2003.
[20] H. A. Shute, D. T. Wilton, D. McA. McKirdy, and D. J. Mapps, "Improved approximations for two-dimensional perpendicular magnetic recording heads," *IEEE Trans. Magn.*, vol. 39, pp. 2098–2102, July 2003.
[21] B. Valcu, T. Roscamp, and H. N. Bertram, "Pulse shape, resolution, and signal-to-noise ratio in perpendicular recording," *IEEE Trans. Magn.*, vol. 38, pp. 288–294, Jan. 2002.
[22] D. T. Wilton, D. McA. McKirdy, H. A. Shute, J. J. Miles, and D. J. Mapps, "Approximate 3-D head fields for perpendicular magnetic recording," *IEEE Trans. Magn.*, vol. 40, pp. 148–156, Jan. 2004.
[23] M. Mallary, A. Torabi, and M. Benakli, "One terabit per square inch perpendicular recording conceptual design," *IEEE Trans. Magn.*, vol. 38, pp. 1719–1724, July 2002.
[24] Y. K. Zheng, D. You, and Y. H. Wu, "Flux-enhanced giant magnetoresistive head design and simulation," *IEEE Trans. Magn.*, vol. 38, pp. 2268–2270, Sept. 2002.
[25] Z. Jin, H. N. Bertram, B. Wilson, and R. Wood, "Simulation of the off-track capability of a one terabit per square inch recording system," *IEEE Trans. Magn.*, vol. 38, pp. 1429–1435, Mar. 2002.
[26] S. Khizroev, Y. Liu, K. Mountfield, M. H. Kryder, and D. Litvinov, "Physics of perpendicular magnetic recording: Writing process," *J. Magn. Magn. Mater.*, vol. 246, pp. 335–344, 2002.
[27] S. K. Khizroev, J. A. Bain, and M. H. Kryder, "Considerations in the design of probe heads for 100 Gbit/in^2 recording density," *IEEE Trans. Magn.*, vol. 33, pp. 2893–2895, Sept. 1997.
[28] J.-G. Zhu, D. Z. Bai, and A. F. Torabi, "The role of SUL in readback and effect on linear density performance for perpendicular recording," *IEEE Trans. Magn.*, vol. 39, pp. 1961–1966, July 2003.